Spatiotemporal Estimation of Daily Peatland Gross Primary Production with Landsat Remote Sensing Data in Germany, Estonia and Finland

Nur Hussain
nurhussain55@gmail.com

Natural Resources Institute Finland: Luonnonvarakeskus

Adrià Descals
CREAF: Centre de Recerca Ecologica i Aplicacions Forestals

Alisa Krasnova
Tartu Ülikool: Tartu Ulikool

Kaido Soosaar
Tartu Ülikool: Tartu Ulikool

Josep Penuelas
CREAF: Centre de Recerca Ecologica i Aplicacions Forestals

Ülo Mander
Tartu Ülikool: Tartu Ulikool

Parvez Rana
Natural Resources Institute Finland: Luonnonvarakeskus https://orcid.org/0000-0002-2578-9680

Research Article

Keywords: Carbon sequestration, Eddy covariance, Gross primary production, Landsat satellite, Peatland ecosystem, Random forest model, Remote sensing

Posted Date: July 3rd, 2026

DOI: https://doi.org/10.21203/rs.3.rs-9832748/v1

Abstract

Peatlands play a central role in the global carbon cycle, particularly in northern latitudes. Hence, monitoring large-scale gross primary production (GPP) in northern peatlands is essential for understanding the impact of climate change on terrestrial carbon sequestration. Few studies have quantified GPP simultaneously across contrasting peatland types and management regimes using remote sensing data. To address this gap, we developed a Landsat-based approach that tracks ecosystem responses across peatland case study areas in Germany, Estonia and Finland that representing natural, drained and restored peatland management regimes. We used a random forest machine-learning model, trained and validated with eddy covariance (EC) flux tower observations, to predict spatial and temporal variability in GPP from Landsat spectral and thermal data. The results demonstrate that Landsat can effectively capture variation in gross GPP across peatland types, including natural, drained, and restored sites. GPP predictions showed good agreement with EC flux tower observations (overall $R^2 \approx 0.57$, RMSE ≈ 3.0 g C m^{-2} d^{-1}), indicating that Landsat-based models capture much of the spatial-temporal variability in productivity across our sites, though site-specific errors vary (R^2 range 0.38–0.69). These findings support the use of satellite-driven approaches for consistent, large-scale monitoring of peatland productivity across different management conditions.

1. Introduction

Peatlands are essential components of terrestrial carbon (C) storage, functioning as long-term C sinks through the accumulation of organic matter under persistently waterlogged conditions (Limpens et al 2008; Knox et al 2017; Loisel and Gallego-Sala 2022). Peatlands cover roughly 3% of the global land surface yet store nearly one-third of the world's soil C stock. This emphasizes their disproportionate role in regulating the climate (Parish et al 2008; Beaulne et al 2021; Ribeiro et al 2021). Peatland vegetation assimilates atmospheric carbon dioxide (CO_2) primarily through gross primary production (GPP), making GPP a key indicator of ecosystem C sequestration (Spielmann et al 2019; Tay et al 2025). Most previous research has focused on individual sites, with findings limited to broader regional scales (Kross et al 2013). Understanding the spatiotemporal patterns of peatland GPP is important for reducing uncertainties in global C budgets and evaluating peatland ecosystem responses to climate variability and land–atmosphere interactions, particularly across boreal, hemiboreal and temperate regions (Kross et al 2013; Junttila et al 2021; Junttila et al 2023; Tong et al 2025).

Peatland GPP and CO_2 fluxes have been extensively investigated using site-level eddy covariance (EC) measurements, which provide continuous, high-frequency observations of net C exchange, from which GPP and ecosystem respiration can be derived through flux partitioning (Kross et al 2013; Krasnova et al 2025; Yildiz et al 2025). EC flux towers provide information on how peatland vegetation responds to key environmental drivers, including solar radiation, air and soil temperatures, water table depth and soil moisture, capturing diurnal, seasonal, and interannual patterns of C uptake (Lees et al. 2021; Yao et al.2022). Most EC flux-based studies have focused on agricultural, forest, and grassland ecosystems, whereas observations of peatlands remain limited (Kross et al 2013; Hurkuck et al 2016). Moreover, EC flux measurements are sensitive to low-turbulence conditions and to uncertainties in flux partitioning. Their ability to represent C exchange across heterogeneous landscapes is also limited by the relatively small spatial footprint of flux towers (Cai et al 2021; Hussain et al 2024b; Yildiz et al 2025). The spatial variability of peatlands, arising from micro-topography, differences in vegetation composition and hydrological gradients, exerts a significant influence on GPP at the landscape scale (Malhotra et al 2016; Xie et al 2023). Integrating EC measurements with spatially extensive and temporally consistent satellite remote sensing observations enables a comprehensive assessment of peatland C uptake across heterogeneous landscapes (Tramontana et al 2016; Walther et al 2018; Isoaho et al 2024). This approach supports large-scale monitoring of CO_2 dynamics and upscaling site-level GPP (Hussain et al 2024a; Ghazaryan et al 2024; Walcker et al 2025).

Remote sensing-based methods can estimate C uptake through GPP at diverse spatial and temporal scales, from individual ecosystems to regional and global extents (Gelybó et al 2013; Sun et al 2019a; Zhu et al 2024; Christiani et al 2024). Among these approaches, the light use efficiency (LUE) model, initially developed by Monteith (1972) and widely applied for satellite-based GPP estimation, relates GPP to the amount of photosynthetically active radiation (PAR) absorbed by vegetation and the efficiency with which it is converted into biomass (Monteith 1972; Xiao et al 2005; Zhang et al 2017; Hussain et al 2024b). Since 1999, the Moderate Resolution Imaging Spectroradiometer (MODIS) has provided global GPP estimates at a spatial resolution of 1 km (MOD17A2), capturing broad spatial and temporal patterns across diverse ecosystems (Running and Zhao 2015). However, satellite-based GPP models for peatlands have received less attention than those developed for major terrestrial ecosystems such as forests, croplands, and grasslands on mineral soils, even though peatlands can be significant C sinks (Lees et al 2021; Balogun et al 2023; Huang et al 2024). Moreover, MODIS often underestimates GPP in natural peatlands and flooded areas due to its coarse spatial resolution (1 km), pixel heterogeneity, limitations in climate input data and assumptions about LUE parameters (Kanniah et al 2009; Gelybó et al 2013; Knox et al 2017). These limitations reduce the accuracy of estimating fine-scale GPP-based C uptake variability in complex peatland ecosystems. In contrast, Landsat-based GPP estimation, with its finer spatial resolution (30 m) and enhanced spectral sensitivity, can provide spatially detailed estimates of peatland GPP than coarse-resolution products such as MODIS (Knox et al 2017; Hussain et al 2024a).

Landsat imagery, incorporating spectral bands and land surface temperature (LST), provides a valuable approach for estimating GPP across spatially heterogeneous peatland landscapes (Fu et al 2014; Sun et al 2019b; Sun et al 2024). Landsat sensors include the thematic mapper (TM), enhanced thematic mapper plus (ETM+), operational land imager (OLI), and operational land imager/thermal infrared sensor (OLI/TIRS). They offer fine spatial resolution and enhanced spectral sensitivity, enabling detailed mapping of spatial patterns in C assimilation across diverse peatland ecosystems. The broad spatial coverage and long-term continuity of Landsat data facilitate the upscaling of site-level GPP measurements to broader landscape extents. In addition, machine learning algorithms, particularly random forest (RF) regression, provide a reliable approach for integrating diverse remote sensing inputs to predict GPP across heterogeneous ecosystem landscapes (Sarkar et al 2022; Lassalle and de Souza Filho 2022; Qian et al 2024; Rhif et al 2025). Most existing studies using machine learning have focused on forest ecosystems (Chen et al 2019b; Chen et al 2019a), agricultural landscapes (Wolanin et al 2019), mangrove ecosystems (Tang et al 2023) and grassland ecosystems (Wang et al 2023). The application of machine learning methods to peatlands remains limited, particularly in spatially heterogeneous boreal and hemiboreal ecosystems at northern latitudes and under contrasting management conditions (Beaver et al 2024).

Peatlands represent one of the most significant terrestrial C reservoirs, storing an estimated 600 Gt of carbon globally (Yu et al 2010; Roberts et al 2025). Their long-term role as C sinks has been increasingly compromised by climate warming and anthropogenic disturbances, particularly across Europe, where centuries of widespread drainage have profoundly transformed peatland hydrology and biogeochemical processes (Giese et al 2025). In boreal and hemi-boreal regions, C cycling is further influenced by forest management practices, as nearly two-thirds of boreal forests are managed, with management intensity being particularly high in Nordic countries (Gauthier et al 2015; Kuuluvainen and Gauthier 2018; de Quesada et al 2025). Consequently, many peatlands have shifted from being C sinks to becoming C-neutral or even C sources. Finland exemplifies this scenario, with peatlands covering approximately 8.8 Mha, nearly one-third of the national land area, including roughly 1 Mha of shallow-peat areas with 4.7 Mha drained for forestry, significantly contributing to soil CO_2 emissions (Forsell et al 2022; Alm et al 2023). Similar trends are observed in Germany, where emissions from peatlands and other organic soils amount to around 53 Mt CO_2e yr^{-1}, representing over 7 % of national greenhouse gas emissions (UBA 2022; Wichmann and Nordt 2024). In Estonia, peatlands cover roughly 22 % of the land area (Tanneberger et al 2017), yet only about 5.5 % remain in a natural or near-natural statedue to extensive drainage and peat extraction over the twentieth century (Paal and Leibak 2011; Karofeld et al 2017). These transformations demonstrate the ncessity for accurate assessment of peatland carbon dynamics to etermine whether managed peatlands function as C sinks, remain C neutral, or act as C sources, and to inform effective mitigation and restoration strategies.

Despite changes in peatland C storage and growing pressures from forest management and environmental change in Finland, Germany, and Estonia, the spatial and temporal dynamics of GPP remain inadequately quantified at landscape and regional scales, particularly in peatlands. This is mainly attributable to the lack of high-resolution observational data required to adequately capture the effects of management practices, particularly clear-cutting and partial-cutting, on peatland C dynamics (Korkiakoski et al 2023). The aim of this study is to quantify the spatiotemporal dynamics of peatland GPP using Landsat satellite data under different management regimes, specifically clear-cutting and partial-cutting. The specific objectives are to (i) evaluate Landsat-based GPP estimates across sites, (ii) analyze the spatial and temporal variability of GPP under different management regimes, and (iii) evaluate the consistency of Landsat-derived predictors. By integrating Landsat remote sensing, EC flux data with RF regression modeling, this study provides a scalable framework for high-resolution GPP estimation. It addresses critical observational gaps in managed peatlands and enhances the capacity to assess C flux responses to forest management and environmental change at landscape-to-regional scales.

2. Materials and methods

2.1 Study sites

This study included four peatland case study sites in three countries: Lettosuo in Finland, Agali-II in Estonia, Anklam and Zarnekow in Germany (Fig. 1). The Lettosuo site is located in southern Finland with geographical coordinates at N60°38.653' E23°57.498', 125 m a.s.l. This site serves as a key research site for investigating greenhouse gas (GHG) fluxes and ecological dynamics within forestry-drained peatland ecosystems. This area is characterized by a managed peatland forest predominantly composed of Scots pine (*Pinus sylvestris* L.) with patches of deciduous vegetation and understory vegetation, including species typical of peatland habitats. The site represents a classic drained peatland ecosystem, which has been subjected to extensive hydrological and ecological modifications over the decades as part of Finland's forestry management practices. Two management regimes were examined at this site: clear-cut and partial-cut.

The Agali-II site is situated in the Järvselja Training and Experimental Forestry District, Estonia, with geographical coordinates at N58°29.088', E27°31.823', 32 m a.s.l. Covering 3.5 ha, it represents a forestry-drained peatland ecosystem dominated by a 40–50-year-old downy birch (Betula pubescens Ehrh.) stand growing on nitrogen-rich peat soil. The site is characteristic of managed drained peatland forests in the boreal region, where drainage has substantially altered hydrological conditions and vegetation structure (Ranniku et al 2024).

The Anklam site (DE-Akm), with geographical coordinates at N53°51.970', E13°41.005', 1 m a.s.l., is located in northeastern Germany. This site represents a managed peatland ecosystem that has undergone significant drainage and agricultural conversion over time. One of the main research focuses on this site is to evaluate the impact of rewetting measures on peatland carbon dynamics. Rewetting, a restoration technique aimed at raising the water table to reduce peat oxidation, is expected to mitigate CO_2 emissions by slowing peat decomposition.

The Zarnekow site (DE-Zrk), with geographical coordinates at N53°52.557', E12°53.341', 0 m a.s.l., is situated in northeastern Germany. This site is a rewetted fen peatland, formerly drained and used for agricultural purposes, but has since been restored as part of efforts aimed at reducing GHG emissions. Located within the Polder Zarnekow region, the site is characterized by rich organic soils with vegetation dominated by wetland plant species, including sedges (*Carex* spp.) and reed grasses (*Phragmites australis* Trin. ex Steud.), which are typical of fen ecosystems.

2.2 In situ GPP data

We computed daily total GPP (hereafter GPP_{FLUX}) from gap-filled EC flux-derived GPP data. Positive values indicate C uptake by the ecosystem. Daily GPP_{FLUX} data were aggregated to annual cumulative. To analyse long-term productivity patterns, daily GPP_{FLUX} values were aggregated to annual cumulative

GPP for each site (Lettosuo 2016–2024, Agali-II 2021–2023, DE-Akm site 2009–2014, and DE-Zrk site 2013–2014). This data set provides a consistent basis for evaluating spatial and temporal variability in carbon assimilation across different peatland sites. We used site-level daily GPP products derived from EC measurements after gap filling and flux partitioning. Although post-processing workflows may have differed slightly among sites, all datasets were based on standard EC processing procedures and were harmonized to daily time steps for analysis.

2.3 Satellite data

We used the spectral and thermal bands from Landsat-5, -7, -8 and – 9 Level-2 (surface reflectance product) for predicting the GPP values and the LST product as the thermal predictor. The spatial resolution of Landsat imagery is 30 m for the spectral bands (Blue, Green, Red, near infrared (NIR), shortwave infrared (SWIR1, SWIR2)) and 60–120 meters depending on the sensor for LST. We created 15-meter radius buffers around all measurement locations to extract the average spectral values with Google Earth Engine (GEE). Although EC flux footprints typically extend over 100–500 m, the smaller buffer was used to capture homogeneous vegetation conditions near the tower while minimizing spectral mixing from adjacent land-cover types. To ensure data quality, images with more than 30% cloud cover were excluded. Additionally, we applied the *Fmask* and the quality assurance (QA) bands integrated in the Landsat products to mask clouds, cloud shadows, and snow-covered pixels.

2.4 GPP model building and validation

We fitted a random forest regression model (Breiman, 2001) for predicting the GPP values for all sites separately and as combined (Fig. 2). Spectral and thermal bands (Blue, Green, Red, NIR, SWIR1, SWIR2, LST) were used as the predictor variables, and GPP calculated from the field measurements were the response variables. We extracted Landsat time-series data for the overlapping pixel at each site using Google Earth Engine (GEE). Then, we kept only the days that coincided with the EC flux tower data. The model was built within the *Caret* package in R-Studio. We used the parameters of 300 trees and one third (1/3) of tries at every split for the dataset. We used a partition of 70% train and 30% test. We trained the Random Forest with the train partition and evaluated the performance of the model with the test partition. We also trained a Random Forest model for each site and cross-validated with the data from the rest of the sites. The accuracy metrics used were the mean error (ME), root-mean-square error (RMSE), and coefficient of determination (R^2). In addition, we used the Gini metric to estimate the importance of each spectral and thermal band to GPP prediction. The variable importance values were scaled 0-100, summing up to 100, with all spectral variables' importance for GPP modeling. Finally, we applied the Random Forest model to predict GPP to Landsat images using GEE.

3 Results

3.1 Model performance

Landsat-based predictions showed good overall agreement with EC-derived GPP observations (overall R^2 ≈ 0.57, RMSE ≈ 3.0 g C m^{-2} d^{-1}; Fig. 3; Table 1), indicating Landsat-based models capture much of the spatial-temporal variability in productivity across our sites, though site-dependent errors vary (R^2 range 0.38–0.69). Model performance was strongest at FI-Let clearcut (R^2=0.72, RMSE = 2.37 g C m^{-2} d^{-1} and FI-Let partialcutting (R^2=0.63, RMSE = 2.77 g C m^{-2} d^{-1}), whereas lower agreement was observed at Agali (R^2=0.29, RMSE = 4.53 g C m^{-2} d^{-1}). Intermediate performance was obtained for DE-Akm (R^2=0.64, RMSE = 3.48 g C m^{-2} d^{-1}) and DE-Zrk (R^2=0.57,, RMSE = 1.67 g C m^{-2} d^{-1}). Predicted GPP generally reproduced the observed seasonal and inter-site variability in tower-derived GPP, although larger deviations between observed and predicted values were evident during periods of high productivity. Mean error (ME) values ranged from − 1.51 to 1.88 g C m^{-2} d^{-1}, indicating relatively limited systematic bias across sites.

Cross-site validation results (Table 1) demonstrated robust model generalization, with mean error, RMSE, and R^2 values supporting consistent performance across sites. The leave-one-site-out validation confirmed that the model is transferable between ecosystems, maintaining stable accuracy even when tested on independent locations. Mean error values (Table 1) indicated site-dependent bias, with underestimation at Agali-II and DE-Zrk and overestimation at DE-Akm and the FI-Let_clearcut site.

Table 1
Cross-site validation accuracy metrics obtained by training a Random Forest regression model with all sites except one site that is left for testing. The metrics represent the mean error (ME), root-mean-squared error (RMSE), and coefficient of determination (R^2). Units for ME and RMSE are g C m^{-2} d^{-1}.

Site	ME	RMSE	R²	n
'Agali-II'	-1.01	2.56	0.69	25
'FI-Let_clearcut'	0.34	2.76	0.61	68
'FI-Let_partialcutting'	-0.40	2.80	0.53	66
'DE-Akm'	0.91	3.66	0.49	18
'DE-Zrk'	-0.64	2.11	0.38	8
'All'	0.37	3.00	0.57	180

Seasonal dynamics of GPP were also well represented by the model (Fig. 4). The seasonality plots illustrate that predicted GPP follows the observed flux tower data closely throughout the growing season, capturing both the onset and decline of photosynthetic activity. Seasonal amplitude differed among sites, with stronger peaks at the Finnish managed sites and lower or more constrained productivity dynamics at the German peatland sites.

An example map of predicted GPP for the Lettosuo site in Finland (Fig. 5) visually demonstrates the spatial distribution of modeled productivity within the site, with higher modeled productivity associated with vegetated areas and lower values in less productive or more open zones. This demonstrates the capacity of the model to produce spatially explicit GPP estimates at Landsat resolution.. The left panel shows a Landsat-8 false color composite (SWIR1–NIR–Red), while the right panel displays the corresponding GPP prediction. The predicted map clearly distinguishes productive vegetated areas from less active zones, confirming the model's potential for regional-scale productivity mapping and monitoring. We also demonstrated the predicted GPP in partial cut and clear-cut management regimes in Finland (Fig. 6).

Predicted GPP differed between the two Finnish management regimes (Fig. 6). The clear-cut area showed stronger seasonal peaks and a more uniform spatial pattern, whereas the partial-cut area displayed lower seasonal amplitude and greater within-site heterogeneity.

3.2 Variable importance

Variables related to NIR reflectance, SWIR bands, and LST exhibited the highest Gini importance values, highlighting their dominant role in explaining GPP variability across sites (Fig. 7).

Predictor importance varied among sites (Fig. 7). NIR and LST consistently ranked among the most important predictors across all sites, whereas the relative contribution of visible and SWIR bands differed by peatland type and management regime. At the Finnish sites, Red and SWIR1 gained importance under clear-cut and partial-cut conditions, while the German sites showed a stronger contribution from Red and SWIR2.

4. Discussion

4.1 Model performance

Our results show that Landsat-based RF models can capture a substantial share of peatland GPP variability across contrasting sites, although predictive performance differed among peatland types and management conditions. Estimating peatland GPP from Landsat imagery depends on the ability of multispectral and thermal signals to reflect ecosystem-scale photosynthetic activity (Gitelson et al 2012; Chen et al 2019b; Cao et al 2025). In this study, we employed the RF to relate Landsat spectral bands (Blue, Green, Red, NIR, SWIR1, SWIR2), and LST to EC flux–derived GPP across different peatland sites. RF is well-suited for peatlands because it models nonlinear relationships and interactions caused by heterogeneous vegetation, variable water content, and management disturbances (Beaver et al 2024; Li et al 2024). This approach leverages NIR reflectance to capture canopy structure, leaf area, and internal scattering, all of which are closely associated with photosynthetic activity (Wu et al 2025; Dashti et al 2025). LST responds to thermal adaptation and surface energy balance, which influence photosynthetic and physiological processes to affect C uptake (Nievola et al 2017; Hussain et al 2026). At the Agali-II site, NIR and LST each contribute about 18% to total Gini importance, showing the collective role of canopy structure and microclimate in regulating GPP in the heterogeneous peatland ecosystem.

Spectral properties of Landsat bands contributions emphasize the unique site conditions and the impact of management practices. At Lettosuo, both clear-cut and partial-cut schemes increased the influence of the Red and SWIR1 bands, due to soil exposure and regenerating vegetation changing reflectance and water-absorption signals. In both sites in Germany, the Red and SWIR2 bands were more pronounced, indicating that vegetation composition, peat moisture, and canopy density modulate the spectral sensitivity of Landsat data to photosynthetic activity (Hislop et al 2018; Wang et al 2022). The practical implication is that while NIR and LST provide broad, transferable predictors, visible and SWIR bands capture local ecological variability, canopy structure changes, and management-induced spectral differences (Harris and Bryant 2009; Hislop et al 2018; Zhang et al 2025). These wavelength response characteristics indicate the need to use multiple spectral bands to capture compositional variability in peatland C uptake measurements accurately.

RF model captured substantial spatiotemporal variation in peatland GPP across the study sites. Among the site-specific cross-validation results, the highest predictive accuracy was observed at Agali-II, whereas performance was lower at DE-Zrk and DE-Akm. Across all sites, the combined RF model retained strong predictive skill, demonstrating the ability of Landsat-based approaches to generalize across countries while remaining sensitive to local ecological and management conditions (Pax-Lenney et al 2001; Zelioli et al 2025). The results are consistent with established controls of peatland GPP, such as canopy structure, thermal regulation, and water availability, and further support the effectiveness of multi-band RF models for accurate, cross-site estimation of productivity (Schaefer et al 2012; Wu et al 2016).

4.2 GPP variability under clear-cut and partial cut management regimes

RF results represented spatial and temporal patterns in peatland GPP closely linked to management regimes, although variability and uncertainty remained across sites (Cai et al 2021; Lees et al 2021). Lettosuo's clear-cut peatlands management regimes demonstrated relatively homogeneous spatial patterns due to simplified canopy structure and reduced vertical complexity (Kettridge et al 2013; Korkiakoski et al 2023). Tree removal likely reduced canopy shading and may have enhanced light penetration to the regenerating understory, thereby simplifying within-pixel spectral composition and improving the relationship between Landsat-derived reflectance and photosynthetic activity (Hussain et al 2024a; Liu et al 2025). However, spatial interpretation, related to rapid colonization by early successional grasses, shrubs, and herbaceous species, produced pronounced seasonal peaks in GPP, reflecting high sensitivity to radiation and temperature (Huenneke et al 2002; Blanco et al 2016; Preston and Fjellheim 2020; Hussain et al 2024a). Open canopy increased the influence of the visible and SWIR bands, as changes in soil exposure and moisture varied the reflectance patterns, accentuating the rational value of these bands in detecting management-induced changes (Blanco et al 2016; Hussain et al 2024a).

Lettosuo partial-cut management regimes retained varying levels of overstory and a heterogeneous understory, with aggregate spatial variability in leaf area, light distribution, and microclimate (Battaglia et al 2002; Bose et al 2014; Leppä et al 2020). This structural heterogeneity introduced spectral complexity within Landsat pixels, slightly reducing predictive performance. The retained canopy regulated light accessibility and surface temperatures, assisting in stabilizing soil moisture and buffering against short-term environmental extremes associated with the thinning shock from the management intervention (Mayer et al 2020; Hussain et al 2024a). Consequently, the seasonal variability of GPP was reduced relative to clear-cut sites, with moderate productivity throughout the growing season. These patterns theoretically reflect the interaction of canopy structure with light, temperature, and water availability, which jointly regulate photosynthesis and C uptake (GOULDEN et al 2011; Mayer et al 2020).

Understanding the drivers of spatial and temporal variability in C uptake is critical for practical peatland management. The observed patterns illustrate that forest management changes the magnitude, distribution, and responsiveness of peatland GPP by changing canopy architecture, understory composition, and soil exposure (ref). From a practical perspective, incorporating knowledge of structural complexity and successional dynamics improves the interpretation of Landsat-derived GPP, enhances model accuracy, and supports robust C accounting in managed peatlands. These results also emphasize the need to consider management-driven heterogeneity when scaling satellite-based productivity estimates across diverse peatland ecosystems.

4.3 Landsat-derived variables performance

Across all study sites, Landsat-derived variables consistently captured the influential controls of peatland GPP, despite differences in vegetation structure, climate and management regimes (Wietecha et al 2025). NIR reflectance and LST consistently appeared as the most influential predictors of peatland GPP, emphasizing their significant role in capturing key ecosystem processes (Harris et al 2015; De Clerck et al 2026). At Agali-II, NIR and LST each accounted for approximately 18% of total predictor importance, underscoring the importance of canopy structure and thermal conditions for GPP estimation at this drained peatland site. NIR reflectance is highly sensitive to canopy structure, leaf area index (LAI), and internal leaf scattering, all of which are closely correlated to the photosynthetic capacity of vegetation (Harris and Dash 2011; Hussain et al 2024b). High NIR values typically indicate dense, healthy vegetation with greater potential for C assimilation, whereas lower values may reflect sparse or stressed canopies (Burdun et al 2023). LST provides the thermal environment experienced by the ecosystem, encompassing surface energy balance and temperature-dependent constraints on photosynthetic activity (Chang et al 2021; Bai et al 2025). Since terrestrial photosynthesis and ecosystem respiration (RE) are strongly temperature-dependent, LST can indicate changes in carbon uptake and use efficiency, particularly under elevated surface temperature conditions (Ensminger et al 2004; Wang et al 2015; Nievola et al 2017; Jiang et al 2025). This relationship not only strengthens the theoretical foundation for linking spectral and thermal signals to ecosystem productivity but also offers practical direction for developing remote sensing–based monitoring frameworks capable of reliably estimating C fluxes across diverse and heterogeneous peatland landscapes.

The contributions of visible (Blue, Green, Red) and SWIR bands varied among sites, reflecting differences in soil exposure, peat moisture, and vegetation composition. This site-specific ecological and management-induced variation is particularly relevant in substantially complex or partially managed peatlands. Multisensor data could provide finer-resolution physiological or structural understanding, and their limited coverage makes multispectral Landsat data a practical choice for large-area GPP monitoring (Crichton et al 2015). Overall, the results confirm that core predictors like NIR and LST are broadly transferable, while secondary bands enhance sensitivity to local heterogeneity and management effects.

4.4 Limitations and future research directions

Despite the strength of Landsat-based RF models, several limitations remain. The 30 m spatial resolution limits the detection of fine-scale heterogeneity in microtopography, vegetation composition, and moisture conditions, particularly in structurally complex peatlands. RF models did not explicitly incorporate physiological, hydrological, or biophysical processes that regulate peatland productivity. Temporal gaps due to cloud cover and the Landsat revisit cycle introduce uncertainty in daily GPP estimates, particularly during periods of rapid phenological change.

Model evaluation was also constrained by the uneven number of matched Landsat-flux observations among sites, with particularly limited samples at DE-Zrk and DE-Akm, which may have reduced the stability of site-specific performance estimates.

Future research should integrate higher-resolution satellite data, such as drone-based observations, to capture fine-scale heterogeneity. Incorporating site-level LUE parameters, continuous soil moisture, water table depth, temperature measurements, and solar-induced chlorophyll fluorescence (SIF) can enhance physiological realism and sensitivity to short-term dynamics. Multisensor fusion combining Landsat, drones, and site-based SIF would reduce uncertainties related to cloud cover, revisit intervals, and spectral limitations, thereby improving temporal and spatial estimates of GPP. Expanding EC flux tower networks across diverse peatland types and management regimes would improve model calibration and transferability. Hybrid approaches that combine machine learning with process-based models of C, water, and energy fluxes would increase interpretability and provide mechanistic understandings into productivity dynamics. Collectively, these strategies would enhance the ecological relevance, accuracy, and operational utility of satellite-derived GPP, supporting improved monitoring and management of peatland C dynamics under clear-cut, partial-cut, and other forest management practices.

5. Conclusion

This study demonstrates the potential of Landsat remote sensing combined with RF modeling to quantify the spatiotemporal dynamics of daily GPP across contrasting peatland and management regimes. By integrating multispectral and thermal Landsat observations with EC flux data from Finland, Estonia, and Germany, we developed a transferable modeling approach capable of capturing spatial and temporal variability in peatland productivity across drained, restored, clear-cut, and partial-cut management scenarios. The Landsat-based models showed good agreement with EC tower-derived GPP across all sites, with consistent performance under different vegetation structures and management intensities. The results indicate that NIR and LST are robust predictors of peatland GPP, reflecting the combined influence of canopy structure, vegetation vigor, and thermal controls on photosynthetic activity. SWIR and visible bands further improved sensitivity to local variability related to peatland management-induced changes in canopy cover. Differences between clear-cut and partial cut management regimes highlight the strong influence of tree structure on peatland carbon uptake. Clear-cut areas exhibited more homogeneous spatial patterns and stronger seasonal responses, whereas partial cut sites showed reduced variability linked to retained canopy cover and microclimatic conditions. These findings emphasize that management practices substantially alter both the magnitude and spatial distribution of peatland GPP, with important implications for C accounting and climate mitigation strategies. Overall, this study fills an important observational gap by providing high-resolution estimates of peatland GPP across multiple case study areas using a consistent remote sensing approach.

Declarations

Competing interests:

The authors have no relevant financial or nonfinancial interests to disclose.

Funding

This study was funded by Horizon Europe project ALFAwetlands (Grant Agreement Number 101056844) and REACTION project (Decision number 367824, Research Council of Finland, Water4All 2023 Joint Transnational Call). This study was also supported by the Estonian Research Council (PRG2032), and the EU through the European Regional Development Fund (Centre of Excellence TK200, AgroCropFuture), by the European Union Horizon programme under grant agreement No 101079192 LiWeFoR (MLTOM23003R) and the European Research Council (ERC) under grant agreement No 101096403 PeatlandN2O (MLTOM23415R).

Author contribution

Nur Hossain: Methodology, Resources, Software, Validation, Visualization, Writing – Original draft. Adrià Descals: Formal analysis, Resources, Software, Validation, Visualization, Validation, Writing – Review & Editing. Alisa Krasnova: Data curation. Kaido Soosaar: Writing – Review & Editing. Josep Penuelas: Writing – Review & Editing. Ülo Mander: Writing – Review & Editing. Parvez Rana: Conceptualization, Funding acquisition, Project administration, Resources, Supervision, Validation, Writing – Review & Editing.

Data Availability

Data are available from the corresponding author upon reasonable request.

References

1. Alm J, Wall A, Myllykangas J-P, et al (2023) A new method for estimating carbon dioxide emissions from drained peatland forest soils for the greenhouse gas inventory of Finland. Biogeosciences 20:3827–3855. doi: 10.5194/bg-20-3827-2023
2. Bai X, Fang J, Liu C, et al (2025) Assessing the cooling effects of vegetation greening on surface temperature under climate warming in China's Loess Plateau. Ecological Engineering 221:107787. doi: 10.1016/j.ecoleng.2025.107787
3. Balogun O, Bello R, Higuchi K (2023) Terrestrial CO2 exchange diagnosis using a peatland-optimized vegetation photosynthesis and respiration model (VPRM) for the Hudson Bay Lowlands. Science of the Total Environment 875:162591. doi: 10.1016/j.scitotenv.2023.162591
4. Battaglia MA, Mou P, Palik B, Mitchell RJ (2002) The effect of spatially variable overstory on the understory light environment of an open-canopied longleaf pine forest. Canadian Journal of Forest Research 32:1984–1991. doi: 10.1139/x02-087
5. Beaulne J, Garneau M, Magnan G, Boucher É (2021) Peat deposits store more carbon than trees in forested peatlands of the boreal biome. Scientific Reports 11:2657. doi: 10.1038/s41598-021-82004-x
6. Beaver J, Humphreys ER, King D (2024) Random Forest Development and Modeling of Gross Primary Productivity in the Hudson Bay Lowlands. Canadian Journal of Remote Sensing. doi: 10.1080/07038992.2024.2355937
7. Blanco LJ, Paruelo JM, Oesterheld M, Biurrun FN (2016) Spatial and temporal patterns of herbaceous primary production in semi-arid shrublands: a remote sensing approach. Journal of Vegetation Science 27:716–727. doi: 10.1111/jvs.12398
8. Bose AK, Harvey BD, Brais S, et al (2014) Constraints to partial cutting in the boreal forest of Canada in the context of natural disturbance-based management: a review. Forestry 87:11–28. doi: 10.1093/forestry/cpt047
9. Breiman L (2001) Random Forests. Machine Learning 45:5–32. doi: 10.1023/A:1010933404324
10. Burdun I, Bechtold M, Aurela M, et al (2023) Hidden becomes clear: Optical remote sensing of vegetation reveals water table dynamics in northern peatlands. Remote Sensing of Environment 296:113736. doi: 10.1016/j.rse.2023.113736
11. Cai Z, Junttila S, Holst J, et al (2021) Modelling daily gross primary productivity with sentinel-2 data in the nordic region–comparison with data from modis. Remote Sensing 13:1–18. doi: 10.3390/rs13030469

12. Cao D, Huang X, Liu G, et al (2025) Evaluating the Performance of Satellite-Derived Vegetation Indices in Gross Primary Productivity (GPP) Estimation at 30 m and 500 m Spatial Resolution. Remote Sensing 17:3291. doi: 10.3390/rs17193291
13. Chang Q, Xiao X, Doughty R, et al (2021) Assessing variability of optimum air temperature for photosynthesis across site-years, sites and biomes and their effects on photosynthesis estimation. Agricultural and Forest Meteorology 298–299:108277. doi: 10.1016/j.agrformet.2020.108277
14. Chen L, Wang Y, Ren C, et al (2019a) Assessment of multi-wavelength SAR and multispectral instrument data for forest aboveground biomass mapping using random forest kriging. Forest Ecology and Management 447:12–25. doi: 10.1016/j.foreco.2019.05.057
15. Chen Y, Shen W, Gao S, et al (2019b) Estimating deciduous broadleaf forest gross primary productivity by remote sensing data using a random forest regression model. Journal of Applied Remote Sensing 13:1. doi: 10.1117/1.jrs.13.038502
16. Christiani P, Rana P, Räsänen A, et al (2024) Detecting Spatial Patterns of Peatland Greenhouse Gas Sinks and Sources with Geospatial Environmental and Remote Sensing Data. Environmental Management 74:461–478. doi: 10.1007/s00267-024-01965-7
17. Crichton KA, Anderson K, Bennie JJ, Milton EJ (2015) Characterizing peatland carbon balance estimates using freely available Landsat ETM+ data. Ecohydrology 8:493–503. doi: 10.1002/eco.1519
18. Dashti H, Chen M, Hao D, Yang X (2025) Canopy Structure Exhibits Linear and Nonlinear Links to Biome-Level Maximum Light Use Efficiency. Ecology Letters. doi: 10.1111/ele.70142
19. De Clerck E, Reyes-Muñoz P, Prikaziuk E, et al (2026) High-spatial-resolution gross primary production estimation from Sentinel-2 reflectance using hybrid Gaussian processes modeling. ISPRS Journal of Photogrammetry and Remote Sensing 232:172–195. doi: 10.1016/j.isprsjprs.2025.11.033
20. de Quesada G, Rautakoski H, Xu J, et al (2025) Carbon dynamics after thinning in two boreal forest sites: Upland and drained peatland. Forest Ecology and Management 595:123024. doi: 10.1016/j.foreco.2025.123024
21. Ensminger I, Sveshnikov D, Campbell DA, et al (2004) Intermittent low temperatures constrain spring recovery of photosynthesis in boreal Scots pine forests. Global Change Biology 10:995–1008. doi: 10.1111/j.1365-2486.2004.00781.x
22. Forsell P, Grönfors K, Kallanto J, et al (2022) Greenhouse gas emissions in Finland 1990 to 2020, National Inventory Report under the UNFCCC and the Kyoto Protocol, Submission to the European Union.
23. Fu D, Chen B, Zhang H, et al (2014) Estimating landscape net ecosystem exchange at high spatial–temporal resolution based on Landsat data, an improved upscaling model framework, and eddy covariance flux measurements. Remote Sensing of Environment 141:90–104. doi: 10.1016/j.rse.2013.10.029

24. Gauthier S, Bernier P, Kuuluvainen T, et al (2015) Boreal forest health and global change. Science 349:819–822. doi: 10.1126/science.aaa9092
25. Gelybó Gy, Barcza Z, Kern A, Kljun N (2013) Effect of spatial heterogeneity on the validation of remote sensing based GPP estimations. Agricultural and Forest Meteorology 174–175:43–53. doi: 10.1016/j.agrformet.2013.02.003
26. Ghazaryan G, Krupp L, Seyfried S, et al (2024) Enhancing peatland monitoring through multisource remote sensing: optical and radar data applications. International Journal of Remote Sensing 45:6372–6394. doi: 10.1080/01431161.2024.2387133
27. Giese L, Baumberger M, Ludwig M, et al (2025) Recent trends in moisture conditions across European peatlands. Remote Sensing Applications: Society and Environment 37:101385. doi: 10.1016/j.rsase.2024.101385
28. Gitelson AA, Peng Y, Masek JG, et al (2012) Remote estimation of crop gross primary production with Landsat data. Remote Sensing of Environment 121:404–414. doi: 10.1016/j.rse.2012.02.017
29. GOULDEN ML, MCMILLAN AMS, WINSTON GC, et al (2011) Patterns of NPP, GPP, respiration, and NEP during boreal forest succession. Global Change Biology 17:855–871. doi: 10.1111/j.1365-2486.2010.02274.x
30. Harris A, Bryant RG (2009) A multi-scale remote sensing approach for monitoring northern peatland hydrology: Present possibilities and future challenges. Journal of Environmental Management 90:2178–2188. doi: 10.1016/j.jenvman.2007.06.025
31. Harris A, Charnock R, Lucas RM (2015) Hyperspectral remote sensing of peatland floristic gradients. Remote Sensing of Environment 162:99–111. doi: 10.1016/j.rse.2015.01.029
32. Harris A, Dash J (2011) A new approach for estimating northern peatland gross primary productivity using a satellite-sensor-derived chlorophyll index. Journal of Geophysical Research: Biogeosciences. doi: 10.1029/2011JG001662
33. Hislop S, Jones S, Soto-Berelov M, et al (2018) Using Landsat Spectral Indices in Time-Series to Assess Wildfire Disturbance and Recovery. Remote Sensing 10:460. doi: 10.3390/rs10030460
34. Huang L, Huang Z, Zhou W, et al (2024) Landsat-based spatiotemporal estimation of subtropical forest aboveground carbon storage using machine learning algorithms with hyperparameter tuning. Frontiers in Plant Science. doi: 10.3389/fpls.2024.1421567
35. Huenneke LF, Anderson JP, Remmenga M, Schlesinger WH (2002) Desertification alters patterns of aboveground net primary production in Chihuahuan ecosystems. Global Change Biology 8:247–264. doi: 10.1046/j.1365-2486.2002.00473.x
36. Hurkuck M, Brümmer C, Kutsch WL (2016) Near-neutral carbon dioxide balance at a seminatural, temperate bog ecosystem. Journal of Geophysical Research: Biogeosciences 121:370–384. doi: 10.1002/2015JG003195
37. Hussain N, Arain MA, Wang S, et al (2024a) Evaluating the effectiveness of different variable retention harvesting treatments on forest carbon uptake using remote sensing. Remote Sensing Applications: Society and Environment 33:101124. doi: 10.1016/j.rsase.2023.101124

38. Hussain N, Gonsamo A, Wang S, Arain MA (2024b) Assessment of spongy moth infestation impacts on forest productivity and carbon loss using the Sentinel-2 satellite remote sensing and eddy covariance flux data. Ecological Processes 13:37. doi: 10.1186/s13717-024-00520-w
39. Hussain N, Saifuzzaman M, Islam D, et al (2026) Spatiotemporal dynamics of carbon, water, and energy balance in Bangladesh using multi-source remote sensing and climate data. Remote Sensing Applications: Society and Environment 41:101847. doi: 10.1016/j.rsase.2025.101847
40. Isoaho A, Ikkala L, Päkkilä L, et al (2024) Multisensor satellite imagery reveals spatiotemporal changes in peatland water table after restoration. Remote Sensing of Environment 306:114144. doi: 10.1016/j.rse.2024.114144
41. Jiang M, Liu L, Liu X, Zou C (2025) Stronger response of vegetation photosynthesis to climate change than greenness in pan-Arctic region: First evidence from SIF satellite observations. Ecological Informatics 90:103312. doi: 10.1016/J.ECOINF.2025.103312
42. Junttila S, Ardö J, Cai Z, et al (2023) Estimating local-scale forest GPP in Northern Europe using Sentinel-2: Model comparisons with LUE, APAR, the plant phenology index, and a light response function. Science of Remote Sensing. doi: 10.1016/j.srs.2022.100075
43. Junttila S, Kelly J, Kljun N, et al (2021) Upscaling northern peatland co2 fluxes using satellite remote sensing data. Remote Sensing 13:1–23. doi: 10.3390/rs13040818
44. Kanniah KD, Beringer J, Hutley LB, et al (2009) Evaluation of Collections 4 and 5 of the MODIS Gross Primary Productivity product and algorithm improvement at a tropical savanna site in northern Australia. Remote Sensing of Environment 113:1808–1822. doi: 10.1016/j.rse.2009.04.013
45. Karofeld E, Jarašius L, Priede A, Sendžikaitė J (2017) On the after-use and restoration of abandoned extracted peatlands in the Baltic countries. Restoration Ecology 25:293–300. doi: 10.1111/rec.12436
46. Kettridge N, Thompson DK, Bombonato L, et al (2013) The ecohydrology of forested peatlands: Simulating the effects of tree shading on moss evaporation and species composition. Journal of Geophysical Research: Biogeosciences 118:422–435. doi: 10.1002/jgrg.20043
47. Knox SH, Dronova I, Sturtevant C, et al (2017) Using digital camera and Landsat imagery with eddy covariance data to model gross primary production in restored wetlands. Agricultural and Forest Meteorology 237–238:233–245. doi: 10.1016/j.agrformet.2017.02.020
48. Korkiakoski M, Ojanen P, Tuovinen JP, et al (2023) Partial cutting of a boreal nutrient-rich peatland forest causes radically less short-term on-site CO2 emissions than clear-cutting. Agricultural and Forest Meteorology. doi: 10.1016/j.agrformet.2023.109361
49. Kross A, Seaquist JW, Roulet NT, et al (2013) Estimating carbon dioxide exchange rates at contrasting northern peatlands using MODIS satellite data. Remote Sensing of Environment 137:234–243. doi: 10.1016/j.rse.2013.06.014
50. Kross A, Seaquist JW, Roulet NT (2016) Light use efficiency of peatlands: Variability and suitability for modeling ecosystem production. Remote Sensing of Environment 183:239–249. doi: 10.1016/j.rse.2016.05.004

51. Kuuluvainen T, Gauthier S (2018) Young and old forest in the boreal: critical stages of ecosystem dynamics and management under global change. Forest Ecosystems. doi: 10.1186/s40663-018-0142-2
52. Lassalle G, de Souza Filho CR (2022) Tracking canopy gaps in mangroves remotely using deep learning. Remote Sensing in Ecology and Conservation 8:890–903. doi: 10.1002/rse2.289
53. Lees KJ, Khomik M, Quaife T, et al (2021) Assessing the reliability of peatland GPP measurements by remote sensing: From plot to landscape scale. Science of the Total Environment. doi: 10.1016/j.scitotenv.2020.142613
54. Leppä K, Korkiakoski M, Nieminen M, et al (2020) Vegetation controls of water and energy balance of a drained peatland forest: Responses to alternative harvesting practices. Agricultural and Forest Meteorology 295:108198. doi: 10.1016/j.agrformet.2020.108198
55. Li Y, Henrion M, Moore A, et al (2024) Factors controlling peat soil thickness and carbon storage in temperate peatlands based on UAV high-resolution remote sensing. Geoderma 449:117009. doi: 10.1016/j.geoderma.2024.117009
56. Limpens J, Berendse F, Blodau C, et al (2008) Peatlands and the carbon cycle: from local processes to global implications – a synthesis. Biogeosciences 5:1475–1491. doi: 10.5194/bg-5-1475-2008
57. Liu X, Moudrý V, Schuldt B, Forkel M (2025) GEDI reveals decline in overstorey and increase in understorey canopy cover of protected forests in Central Europe since 2019. Forest Ecology and Management 597:123155. doi: 10.1016/j.foreco.2025.123155
58. Loisel J, Gallego-Sala A (2022) Ecological resilience of restored peatlands to climate change. Communications Earth & Environment 3:208. doi: 10.1038/s43247-022-00547-x
59. Malhotra A, Roulet NT, Wilson P, et al (2016) Ecohydrological feedbacks in peatlands: an empirical test of the relationship among vegetation, microtopography and water table. Ecohydrology 9:1346–1357. doi: 10.1002/eco.1731
60. Mayer M, Prescott CE, Abaker WEA, et al (2020) Tamm Review: Influence of forest management activities on soil organic carbon stocks: A knowledge synthesis. Forest Ecology and Management 466:118127. doi: 10.1016/j.foreco.2020.118127
61. Monteith JL (1972) Solar Radiation and Productivity in Tropical Ecosystems. The Journal of Applied Ecology 9:747. doi: 10.2307/2401901
62. Nievola CC, Carvalho CP, Carvalho V, Rodrigues E (2017) Rapid responses of plants to temperature changes. Temperature 4:371–405. doi: 10.1080/23328940.2017.1377812
63. Paal J, Leibak E (2011) Estonian mires: Inventory of habitats: Publication of the Project 'Estonian mires inventory completion for maintaining biodiversity.
64. Parish F, Sirin A, Charman D, et al (2008) Assessment on peatlands, biodiversity, and climate change. Global Environment Centre & Wetlands International, Wageningen
65. Pax-Lenney M, Woodcock CE, Macomber SA, et al (2001) Forest mapping with a generalized classifier and Landsat TM data. Remote Sensing of Environment 77:241–250. doi: 10.1016/S0034-4257(01)00208-5

66. Prakash Sarkar D, Uma Shankar B, Ranjan Parida B (2022) Machine learning approach to predict terrestrial gross primary productivity using topographical and remote sensing data. Ecological Informatics. doi: 10.1016/j.ecoinf.2022.101697
67. Preston JC, Fjellheim S (2020) Understanding Past, and Predicting Future, Niche Transitions based on Grass Flowering Time Variation. Plant Physiology 183:822–839. doi: 10.1104/pp.20.00100
68. Qian L, Yu X, Zhang Z, et al (2024) Assessing and improving the high uncertainty of global gross primary productivity products based on deep learning under extreme climatic conditions. Science of The Total Environment 957:177344. doi: 10.1016/j.scitotenv.2024.177344
69. Ranniku R, Mander Ü, Escuer-Gatius J, Schindler T, Kupper P, Sellin A, Soosaar K (2024) Dry and wet periods determine stem and soil greenhouse gas fluxes in a drained peatland forest. Science of the Total Environment 928:172452. doi: 10.1016/j.scitotenv.2024.172452
70. Rhif M, Martínez B, Ben Abbes A, Farah IR (2025) Gross primary production prediction and future projection: motivations, challenges, and new directions. Carbon Fluxes and Biophysical Variables from Earth Observation. Elsevier, pp 333–356
71. Ribeiro K, Pacheco FS, Ferreira JW, et al (2021) Tropical peatlands and their contribution to the global carbon cycle and climate change. Global Change Biology 27:489–505. doi: 10.1111/gcb.15408
72. Roberts H, Andrews L, Słowiński M, et al (2025) Holocene Land-Use and Climate Forcing of Ombrotrophic Peatland Dynamics in Northwest Estonia. Journal of Geophysical Research: Biogeosciences. doi: 10.1029/2025JG009140
73. Running SW, Zhao M (2015) User's Guide Daily GPP and Annual NPP (MOD17A2/A3) Products NASA Earth Observing System MODIS Land Algorithm.
74. Schaefer K, Schwalm CR, Williams C, et al (2012) A model-data comparison of gross primary productivity: Results from the North American Carbon Program site synthesis. Journal of Geophysical Research: Biogeosciences. doi: 10.1029/2012JG001960
75. Spielmann FM, Wohlfahrt G, Hammerle A, et al (2019) Gross Primary Productivity of Four European Ecosystems Constrained by Joint CO 2 and COS Flux Measurements. Geophysical Research Letters 46:5284–5293. doi: 10.1029/2019GL082006
76. Sun Z, An Y, Kong J, et al (2024) Exploring the spatio-temporal patterns of global mangrove gross primary production and quantifying the factors affecting its estimation, 1996–2020. Science of The Total Environment 908:168262. doi: 10.1016/j.scitotenv.2023.168262
77. Sun Z, Wang X, Zhang X, et al (2019a) Evaluating and comparing remote sensing terrestrial GPP models for their response to climate variability and CO 2 trends. Science of the Total Environment 668:696–713. doi: 10.1016/j.scitotenv.2019.03.025
78. Sun Z, Wang X, Zhang X, et al (2019b) Evaluating and comparing remote sensing terrestrial GPP models for their response to climate variability and CO2 trends. Science of The Total Environment 668:696–713. doi: 10.1016/j.scitotenv.2019.03.025

79. Tang Y, Li T, Yang X, et al (2023) Mango-GPP: A Process-Based Model for Simulating Gross Primary Productivity of Mangrove Ecosystems. Journal of Advances in Modeling Earth Systems. doi: 10.1029/2023MS003714
80. Tanneberger F, Tegetmeyer C, Busse S, et al (2017) The peatland map of Europe. Mires and Peat 19:22. doi: 10.19189/MAP.2016.OMB.264
81. Tay C, Jovani-Sancho AJ, Yulianti L, et al (2025) Satellite radar advances carbon emissions accountability over tropical peat. Communications Earth & Environment 6:971. doi: 10.1038/s43247-025-02926-6
82. Tong CHM, Peichl M, Noumonvi KD, et al (2025) The Carbon Balance of a Rewetted Minerogenic Peatland Does Not Immediately Resemble That of Natural Mires in Boreal Sweden. Global Change Biology. doi: 10.1111/gcb.70169
83. Tramontana G, Jung M, Schwalm CR, et al (2016) Predicting carbon dioxide and energy fluxes across global FLUXNET sites with regression algorithms. Biogeosciences 13:4291–4313. doi: 10.5194/bg-13-4291-2016
84. UBA (2022) Submission under the United Nations Framework Convention on Climate Change and the Kyoto Protocol 2022: National Inventory Report for the German Greenhouse Gas Inventory 1990–2020.
85. Walcker R, Le Lay C, Gandois L, et al (2025) High-resolution mapping of peatland CO2 fluxes using drone multispectral images. Ecological Informatics 86:103060. doi: 10.1016/j.ecoinf.2025.103060
86. Walther S, Guanter L, Heim B, et al (2018) Assessing the dynamics of vegetation productivity in circumpolar regions with different satellite indicators of greenness and photosynthesis. Biogeosciences 15:6221–6256. doi: 10.5194/bg-15-6221-2018
87. Wang M, Zheng Y, Huang C, et al (2022) Assessing Landsat-8 and Sentinel-2 spectral-temporal features for mapping tree species of northern plantation forests in Heilongjiang Province, China. Forest Ecosystems 9:100032. doi: 10.1016/j.fecs.2022.100032
88. Wang S, Tuya H, Zhang S, et al (2023) Random forest method for analysis of remote sensing inversion of aboveground biomass and grazing intensity of grasslands in Inner Mongolia, China. International Journal of Remote Sensing 44:2867–2884. doi: 10.1080/01431161.2023.2210724
89. Wang X, Li G, Liu L, et al (2015) Effects of extreme temperatures on cause-specific cardiovascular mortality in China. International Journal of Environmental Research and Public Health 12:16136–16156. doi: 10.3390/ijerph121215042
90. Wichmann S, Nordt A (2024) Unlocking the potential of peatlands and paludiculture to achieve Germany’s climate targets: obstacles and major fields of action. Frontiers in Climate. doi: 10.3389/fclim.2024.1380625
91. Wietecha M, Kopeć D, Niedzielko J, et al (2025) Local scale assessment of peatland restoration priorities using multisensor airborne remote sensing and machine learning. Ecological Indicators 180:114366. doi: 10.1016/j.ecolind.2025.114366

92. Wolanin A, Camps-Valls G, Gómez-Chova L, et al (2019) Estimating crop primary productivity with Sentinel-2 and Landsat 8 using machine learning methods trained with radiative transfer simulations. Remote Sensing of Environment 225:441–457. doi: 10.1016/j.rse.2019.03.002
93. Wu C, Yang T, Cheng M, et al (2025) Multi-scale estimation of photosynthetic capacity in larch forests using UAV hyperspectral data: From leaf to canopy. Science of Remote Sensing 11:100220. doi: 10.1016/j.srs.2025.100220
94. Wu Y, Verseghy DL, Melton JR (2016) Integrating peatlands into the coupled Canadian Land Surface Scheme (CLASS) v3.6 and the Canadian Terrestrial Ecosystem Model (CTEM) v2.0. Geoscientific Model Development 9:2639–2663. doi: 10.5194/gmd-9-2639-2016
95. Xiao X, Zhang Q, Saleska S, et al (2005) Satellite-based modeling of gross primary production in a seasonally moist tropical evergreen forest. Remote Sensing of Environment 94:105–122. doi: 10.1016/j.rse.2004.08.015
96. Xie X, Chen JM, Yuan W, et al (2023) A Practical Algorithm for Correcting Topographical Effects on Global GPP Products. Journal of Geophysical Research: Biogeosciences. doi: 10.1029/2023JG007553
97. Yao H, Peng H, Hong B, et al (2022) Environmental Controls on Multi-Scale Dynamics of Net Carbon Dioxide Exchange From an Alpine Peatland on the Eastern Qinghai-Tibet Plateau. Frontiers in Plant Science. doi: 10.3389/fpls.2021.791343
98. Yildiz K, Okiti I, Tamm I, et al (2025) Carbon balance in an abandoned peat extraction area influenced by spatial heterogeneity and vegetation development. Agricultural and Forest Meteorology 375:110872. doi: 10.1016/j.agrformet.2025.110872
99. Yu Z, Loisel J, Brosseau DP, et al (2010) Global peatland dynamics since the Last Glacial Maximum. Geophysical Research Letters. doi: 10.1029/2010GL043584
100. Zelioli L, Farahnakian F, Middleton M, et al (2025) Peatland pixel-level classification via multispectral, multiresolution and multisensor data using convolutional neural network. Ecological Informatics 90:103233. doi: 10.1016/j.ecoinf.2025.103233
101. Zhang Y, Fan Z, Yan W, et al (2025) A Practical Method for Red-Edge Band Reconstruction for Landsat Image by Synergizing Sentinel-2 Data with Machine Learning Regression Algorithms. Sensors 25:3570. doi: 10.3390/s25113570
102. Zhang Y, Xiao X, Wu X, et al (2017) A global moderate resolution dataset of gross primary production of vegetation for 2000-2016. Scientific data 4:170165. doi: 10.1038/sdata.2017.165
103. Zhu W, Xie Z, Zhao C, et al (2024) Remote sensing of terrestrial gross primary productivity: a review of advances in theoretical foundation, key parameters and methods. GIScience and Remote Sensing. doi: 10.1080/15481603.2024.2318846

Figures

Figure 1

Geographic location of the four peatland case study sites representing contrasting peatland conditions and management regimes in Finland, Estonia, and Germany.

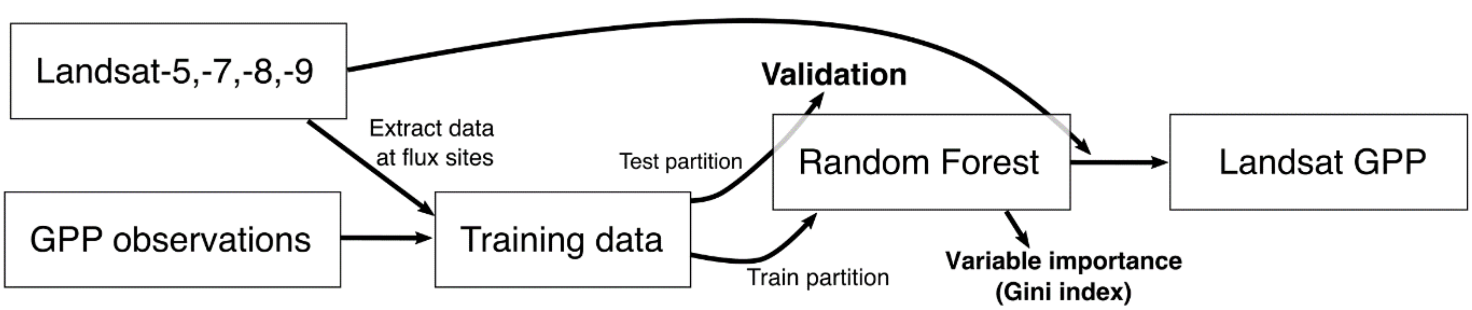

Figure 2

Methodological flowchart illustrating the workflow sequence from data acquisition, through processing, analysis, and output generation.

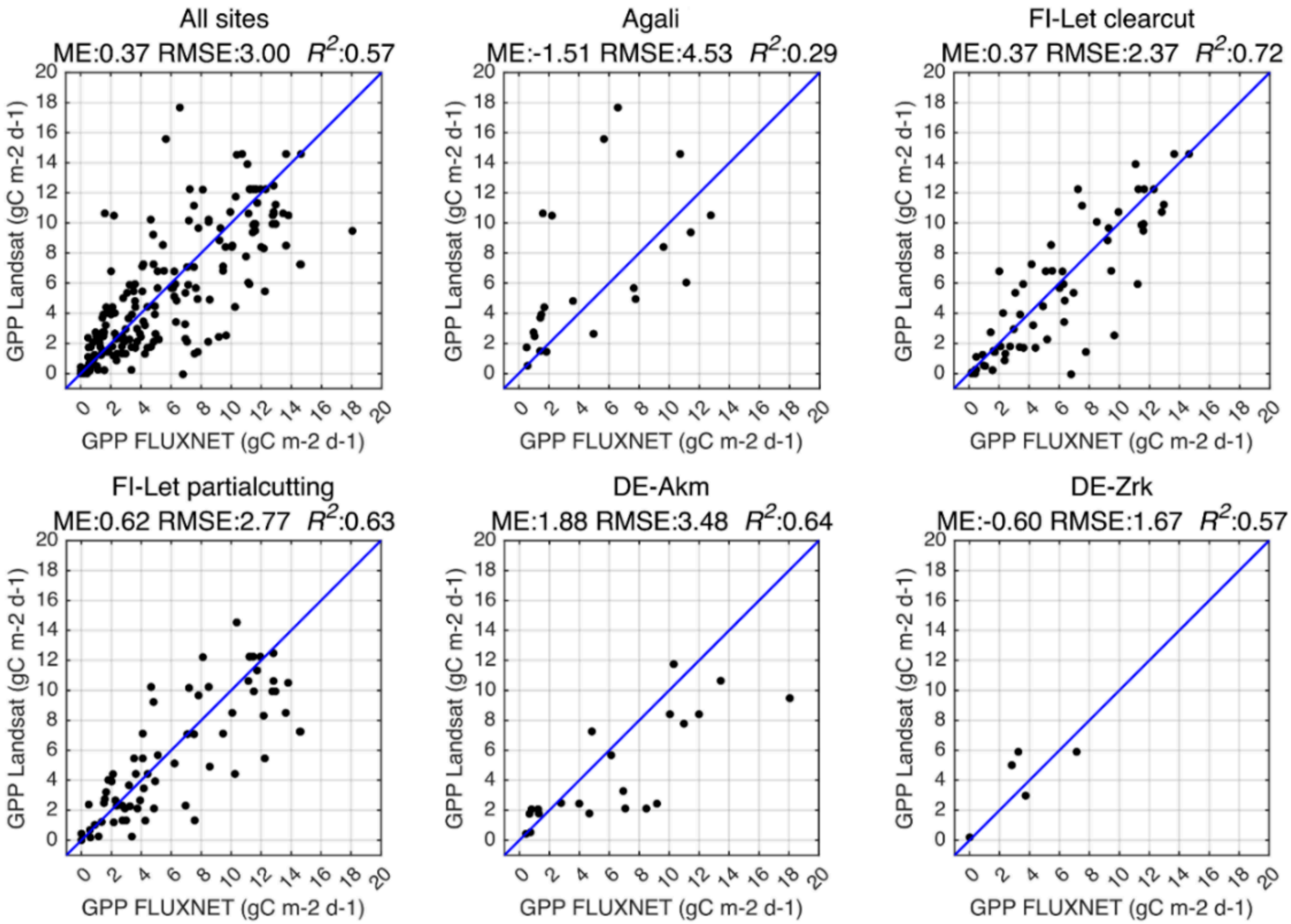

Figure 3

Comparison between GPP observed in the flux towers and GPP predicted with Landsat. Titles of the plots indicate the mean error (ME), root-mean-square error (RMSE), and coefficient of determination (R^2). Units for ME and RMSE are g C m^{-2} d^{-1}.

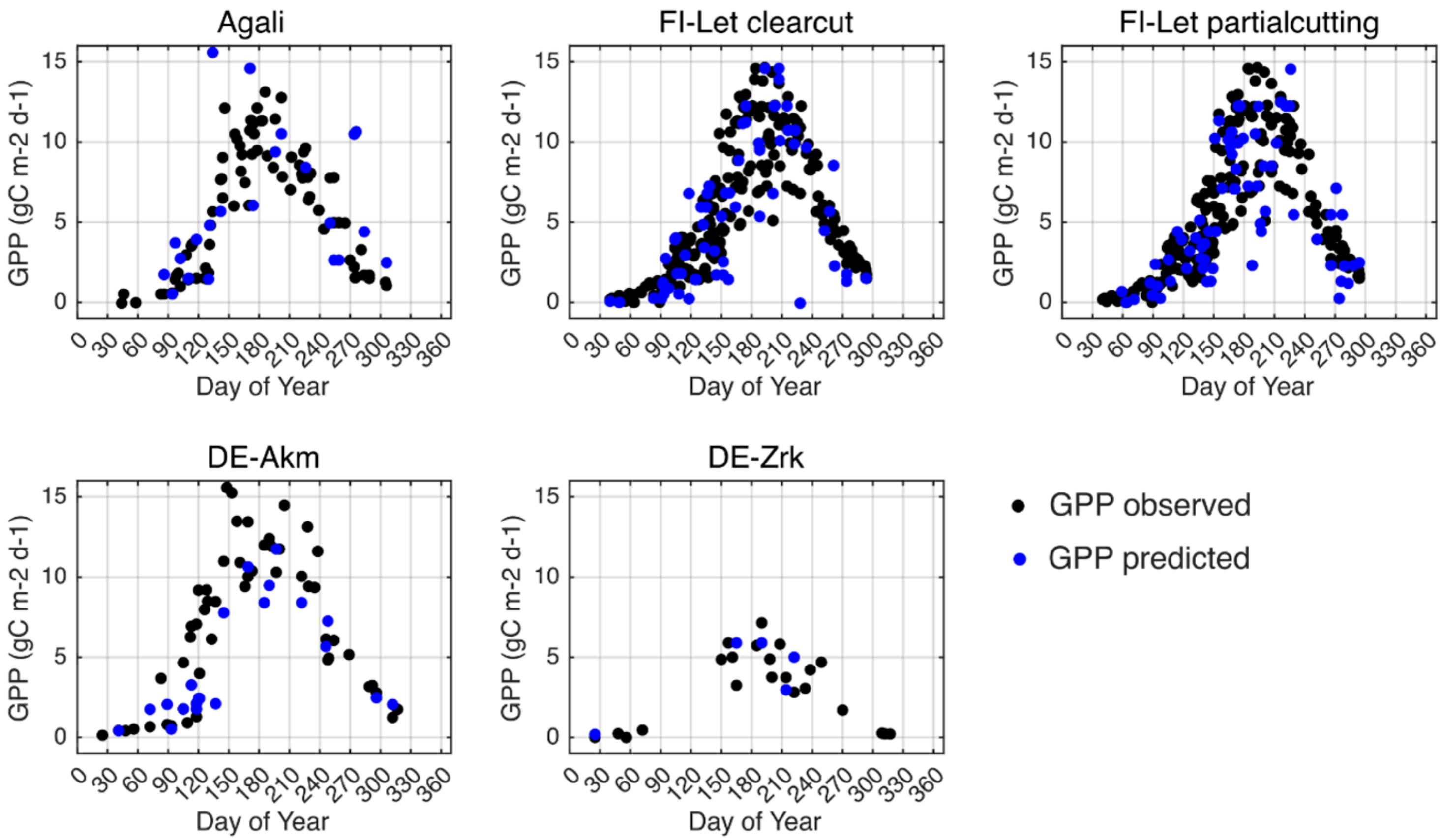

Figure 4

GPP seasonality in each site. Black dots represent all GPP measurements in the sites, while blue dots represent the predicted GPP only for the measurements used for testing the model performance.

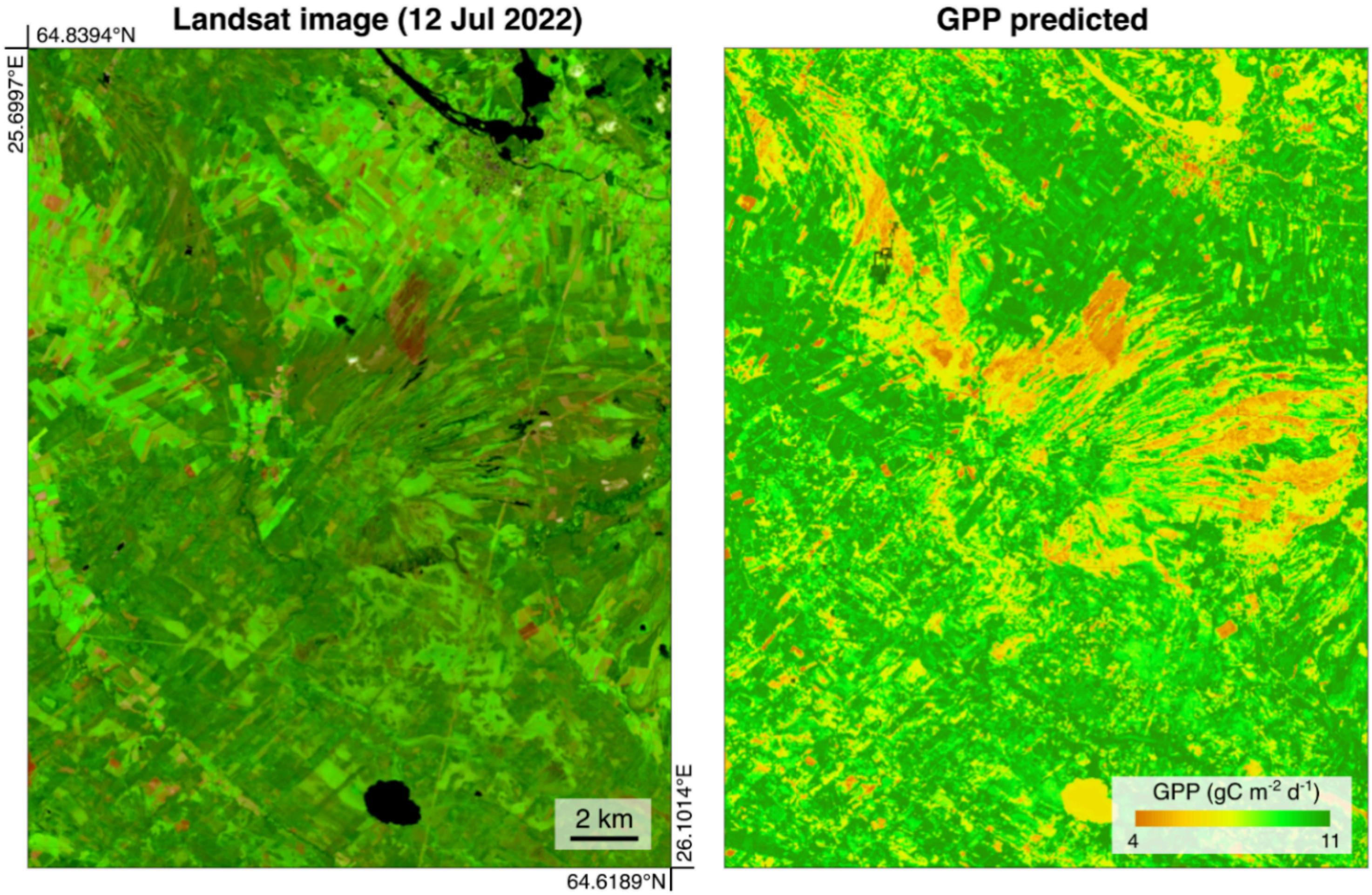

Figure 5

Example of Landsat-based predicted GPP at the Lettosuo site in southern Finland. The left image shows a false color composite (SWIR1-NIR-Red) from Landsat-8 and the right image shows the corresponding predicted GPP.

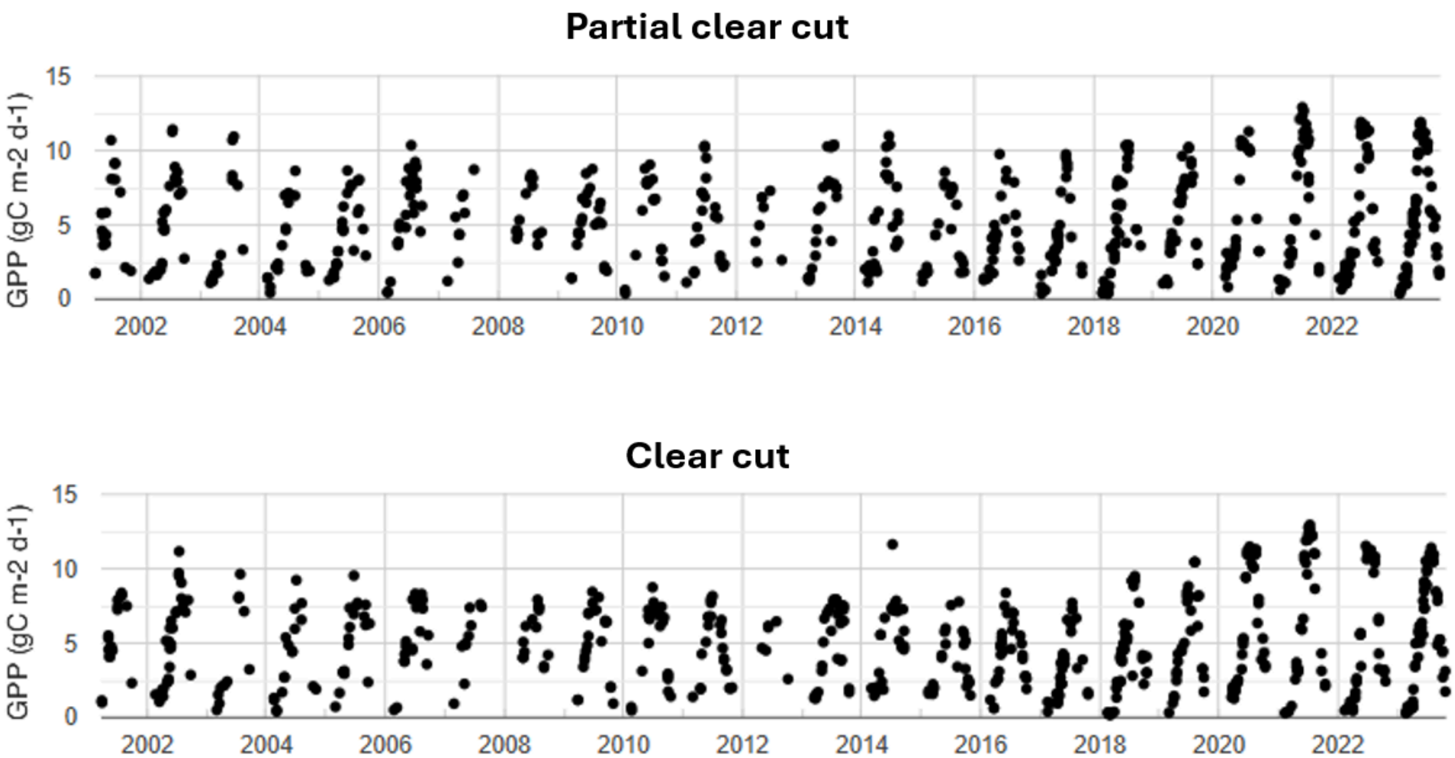

Figure 6

Predicted GPP in partial cut and clear-cut management regimes in Finland.

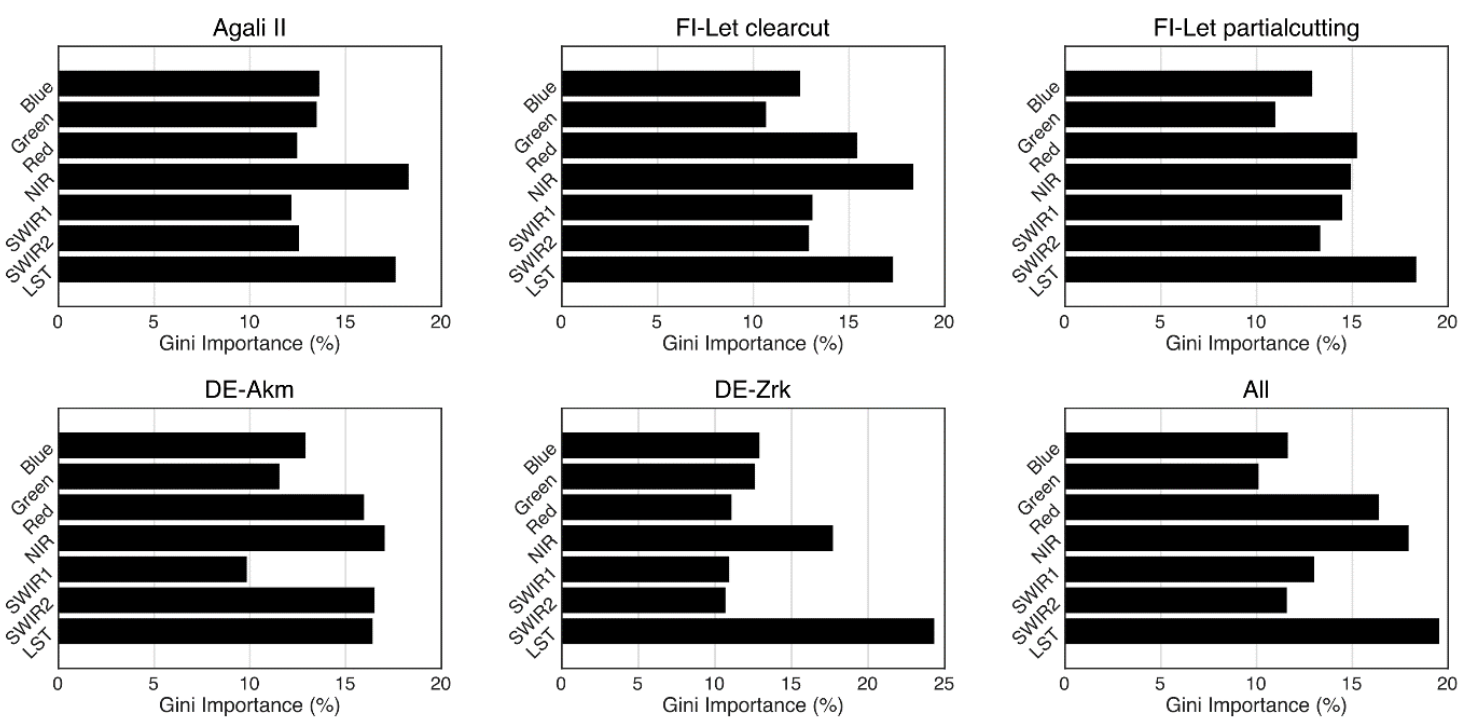

Figure 7

Results of the variable selection based on the Gini importance. The variable importance was obtained by training separate Random Forest models in each site.